Nanoscale

COMMUNICATION

View Article Online
View Journal | View Issue

Magnetoresistive polyaniline/multi-walled carbon nanotube nanocomposites with negative permittivity†

Cite this: *Nanoscale*, 2014, **6**, 181

Received 7th August 2013
Accepted 20th September 2013

DOI: 10.1039/c3nr04152b

www.rsc.org/nanoscale

Hongbo Gu,[ab] Jiang Guo,[bc] Qingliang He,[bc] Yuan Jiang,[b] Yudong Huang,*[a] Neel Haldolaarachige,[e] Zhiping Luo,[d] David P. Young,[e] Suying Wei*[bc] and Zhanhu Guo*[b]

Contrary to the observed positive giant magnetoresistance (GMR) in as-received multi-walled carbon nanotubes (MWNTs), pure polyaniline (PANI) synthesized with Cr(VI) as oxidant and MWNTs/PANI nanocomposites with ammonium persulfate (APS) as oxidant, a room temperature negative GMR of around −2% was reported in MWNTs/PANI nanocomposites with Cr(VI) as oxidant. Different from a frequency switch of permittivity from negative to positive in MWNTs/PANI nanocomposites with APS as oxidant, unique negative permittivity was observed in MWNTs/PANI nanocomposites with Cr(VI) as oxidant within the measured frequency range from 20 to 2×10^6 Hz. The obtained unique negative permittivity was explained by the plasma frequency from the Drude model, at which the permittivity changes from negative to positive and the material changes from a metamaterial to an ordinary dielectric medium. The observed positive and negative GMR behaviors in these disordered systems as verified by the temperature dependent resistivity exploration were well explained through a wave-function shrinkage model and orbital magnetoconductivity theory by calculating the changed localization length (a_0).

The traditional giant magnetoresistance (GMR) effect was observed in multilayer metallic materials consisting of a pair of ferromagnetic layers separated by a non-magnetic metal layer.[1] Recently, GMR effects have been reported in carbon based materials including carbon nanotubes (CNTs) and graphene, and organic semiconductors (OSCs).[2–4] Especially, the GMR effects in CNT systems, conducting polymers and their nanocomposites have gained much attention. For example, 20% GMR at 8 K is reported in a hybrid system containing stacked Co-SWNT (single-walled carbon nanotube)-Fe;[5] up to 300% GMR is observed in a non-magnetic supramolecular spin valve consisting of a SWNT contacted with non-magnetic electrodes and coupled through supramolecular interactions to bisphthalocyaninatoterbium(III) complex ($TbPc_2$) single molecule magnets by reversing the magnetic field at temperatures lower than 1 K; 53 and 65.6% room temperature GMR is observed in pure polyaniline (PANI) doped with *p*-toluenesulfonic acid (PTSA)[6] and phosphoric acid (H_3PO_4),[7] respectively; around 95 and 20% room temperature GMR are observed in 30 wt% Fe_3O_4/PANI[6] and 20 wt% $BaTiO_3$/PANI[8] nanocomposites synthesized by the surface initiated polymerization (SIP) method; and a room temperature GMR of around 35% is observed in 20 wt% $BaTiO_3$/PANI nanocomposites prepared from simple physical mixtures of PANI and $BaTiO_3$ powders.[8] CNTs/PANI nanocomposites have also been investigated for their GMR behavior,[9] electrochemical energy storage,[10] specific DNA sequence detection[11] and hydrogen storage.[12] For example, a positive room temperature GMR of around 15% is reported in 5 wt% MWNTs/PANI nanocomposites synthesized with ammonium persulfate (APS) as oxidant.[9] Recently, Gu *et al.*[13] have reported hexavalent chromium (Cr(VI)) as a strong oxidant to prepare MWNTs/PANI nanocomposites, which served as nanofillers to enhance the tensile strength (about 80%) of the epoxy matrix through strong chemical bonds formed between MWNTs and epoxy *via* the bridging effect of the coated PANI on the MWNT surface.

Metamaterials, historically known as artificially constructed materials with unusual electromagnetic properties,[14] have gained recent attention due to their unique negative refractive index, *i.e.* negative permittivity and/or negative permeability at a given frequency of radiation for cloaking and invisibility applications.[15,16] Recently, the term "metacomposites" has been introduced to describe nanocomposites with negative permittivity, which have potential applications for cloaking,

[a]*School of Chemical Engineering and Technology, Harbin Institute of Technology, Harbin, Heilongjiang 150001, China. E-mail: huangyd@hit.edu.cn*

[b]*Integrated Composites Lab (ICL), Dan F. Smith Department of Chemical Engineering, Lamar University, Beaumont, TX 77710, USA. E-mail: zhanhu.guo@lamar.edu; suying.wei@lamar.edu; Tel: +1 409 880-7654; +1 409 880 7976*

[c]*Department of Chemistry and Biochemistry, Lamar University, Beaumont, TX 77710, USA*

[d]*Department of Chemistry and Physics and Southeastern North Carolina Regional Microanalytical and Imaging Consortium, Fayetteville State University, Fayetteville, NC 28301, USA*

[e]*Department of Physics and Astronomy, Louisiana State University, Baton Rouge, LA 70803, USA*

† Electronic supplementary information (ESI) available. See DOI: 10.1039/c3nr04152b

superlens, wave filters, subwavelength imaging, remote aerospace and superconductors.[6,9,17]

It will be academically interesting and technically important to understand the GMR behaviors and dielectric properties of MWNTs/PANI nanocomposites formed from different oxidants. Meanwhile, negative MR, which means a reduced resistance after applying a magnetic field to the materials, is beneficial for the design of electronic devices with a reduced resistivity after applying an external magnetic field. However, the dielectric permittivity and GMR behaviors of Cr(VI) oxidized MWNTs/PANI nanocomposites have not been reported so far.

Here, unique negative permittivity and negative magnetoresistance (MR) are first reported in disordered conductive MWNTs/PANI nanocomposites with Cr(VI) as oxidant. Meanwhile, a positive MR is observed in as-received MWNTs, pure PANI synthesized using Cr(VI), and MWNTs/PANI nanocomposites prepared with ammonium persulfate (APS) as oxidant. All these are in contrast to the reported results from literature, in which only positive MR (around 15%) is reported.[9] The MR behavior of these nanocomposites is theoretically analyzed based on the wave-function shrinkage model and orbital magnetoconductivity theory. The MWNTs/PANI nanocomposites were synthesized by a surface initiated polymerization (SIP) method. Briefly, MWNTs/PANI nanocomposites with MWNT loadings of 5.0, 10.0 and 20.0 wt% synthesized using Cr(VI) as oxidant are named as T5, T10 and T20, respectively. Aniline was further polymerized on T20 with APS as oxidant and the loading of T20 in the final nanocomposites was controlled at 5.0 wt%, which was named as T205. The aniline was further polymerized on T20 by Cr(VI) and the loading of T20 in the final nanocomposites was 5.0 wt% (the product was named as TCr205). Meanwhile, nanocomposites containing 5.0 wt% MWNTs were also prepared by oxidizing aniline with APS (the product was named as TA05) for comparison. The MWNTs loading in these nanocomposites was calculated based on the weight of aniline monomers. The synthesized nanocomposites in this work are shown in Scheme 1. The details for the nanocomposites synthesis are reported in the ESI.†

The nanocomposites exhibit very different morphology, Fig. 1, from the as-received MWNTs with randomly entangled network, Fig. S1a.† However, the network structure of the MWNTs is still observed in the T5 sample with an average diameter of about 43.4 nm with a deviation of 9%, Fig. 1a, which is thicker than that of the as-received MWNTs. The average diameter of the T20 sample is about 18.5 nm with a deviation of 11%, Fig. S1b.† The wire rather than tube structure is observed in the T205 and TCr205 samples, Fig. S1c and d,† and the average diameter of the nanotubes increases dramatically (around 100 nm) compared with that of the T20 sample, indicating the further polymerization of aniline on the surface of MWNTs. The average diameter of the TA05 sample, Fig. 1b, is also around 100 nm, which is much thicker than that of the as-received MWNTs. The Cr(VI) oxidized pure PANI shows a ball-like morphology, Fig. S1e,† similar to APS oxidized PANI.[6] The TEM images of the MWNTs/PANI nanocomposites show a multilayer morphology and the surface is relatively rough, Fig. S2.† The PANI coating can be obviously observed outside the multi-walls of the MWNTs. The observed PANI coating in the T20 sample, Fig. S2c,† is thinner than that in the T5 sample, Fig. S2b.†

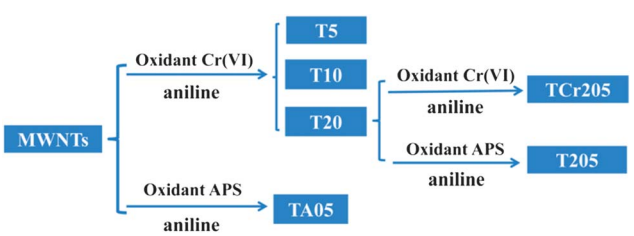

Scheme 1 The polyaniline nanocomposites synthesized in this work.

The characteristic peaks of PANI observed at 1560, 1470, 1285, 1234, 1114 and 782 cm^{-1} in pure PANI synthesized by Cr(VI), T205, and TA05 samples; 1556, 1471, 1289, 1221, 1110, and 779 cm^{-1} in the T5, T10 and T20 samples, Fig. S3A and B† FT-IR spectra, indicate that the synthesized PANI is in the half-oxidized form, *i.e.* "emeraldine" (EB) salt form.[18] However, for the TCr205 sample, Fig. S3A-e,† a different peak at around 1119 cm^{-1} corresponds to the "pernigraniline" (PB) form of PANI.[18] The absorption peaks at 1560 and 1470 cm^{-1} for pure PANI, Fig. S3A-b,† correspond to the C=C stretching vibrations of the quinoid and benzenoid rings in PANI, respectively.[19] Normally, the protonated nitrogen is favorably originated from the imine groups in the PANI chains because the pK_a of the imine group is 5.5 compared to 2.5 for the amine group.[18] Thus, the lower intensity ratio of the quinoid band relative to the benzenoid band in PANI indicates the relatively higher doping level is obtained.[20] The high resolution XPS spectra of pure PANI synthesized with Cr(VI) as oxidant, Fig. S3C,† indicate that the Cr(VI) has been reduced to Cr(III) after oxidation of aniline to form PANI. Fig. 1c shows the Raman spectra of the as-received MWNTs, T5, T205 and TA05 nanocomposites with 785 nm laser excitation. In the typical Raman spectrum of the MWNTs, the G-band (E_{2g} symmetry, graphite mode) appearing at around 1580 cm^{-1} is due to the sp^2 carbon networks,[21] and the characteristic defect induced D band at around 1300 cm^{-1} arises from the sp^3 carbon networks.[22] The integrated intensity ratio of I_D/I_G for the D band and G band has been used to characterize the defect quantity in graphitic materials.[21] The shifts of the G-band from 1584 cm^{-1} of the as-received MWNTs to 1580, 1578 and 1574 cm^{-1} for T5, T205 and TA05 indicate a strong interaction between the MWNTs and the hosting PANI.[23,24] Due to the limited available information about pure PANI synthesized by Cr(VI) from the Raman spectra with 785 nm laser excitation, Fig. S3D,† the Raman spectra of pure PANI synthesized by Cr(VI) and T10 samples with 633 nm laser excitation were recorded, Fig. 1d. The observed four characteristic bands at 1170, 1347, 1476 and 1592 cm^{-1} for pure PANI synthesized by Cr(VI) correspond to the C–H in-plane bending deformation, C=N stretching deformation, C–C and C=C stretching of the benzoid rings of PANI, respectively.[25] In the Raman spectrum of the T10 nanocomposites, the observed bands at 1159 and 1463 cm^{-1} correspond to the characteristic peaks of PANI, and the shift indicates an interaction between the MWNTs and the

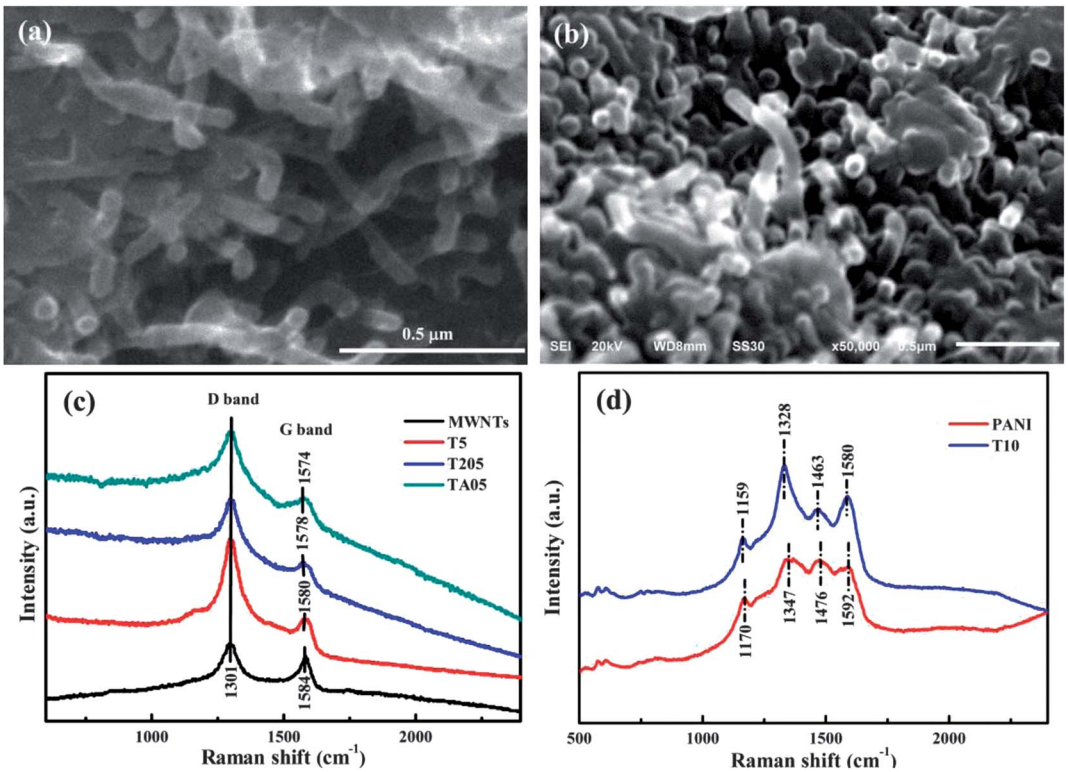

Fig. 1 SEM images of (a) T5 and (b) TA05; Raman spectra of (c) as-received MWNTs, T5, T205 and TA05 with 785 nm laser excitation, and (d) pure PANI synthesized using Cr(VI) and T10 with 633 nm laser excitation.

hosting PANI. The strong bands at 1328 and 1580 cm^{-1} are attributed to the D band and G band of MWNTs, which are overlapped with the PANI bands of 1347 and 1592 cm^{-1}.

Fig. 2 depicts the real permittivity (ε'), imaginary permittivity (ε'') and dielectric loss (tan δ, where tan $\delta = \varepsilon''/\varepsilon'$) as a function of the frequency for pure PANI synthesized by Cr(VI) and its MWNTs nanocomposites at room temperature. All the samples show a frequency dependent permittivity. Pure PANI synthesized by Cr(VI) shows a positive ε' value (from 4875 to 78) within the measured frequency range (20–2 $\times$ 10^6 Hz) and the ε' decreases with increasing frequency, Fig. 2a. The high positive ε' indicates that the mobile charges are no longer free and localized in each metallic island (the metallic island is a well-ordered polymer chain region caused by the oxidation or protonation. Generally, the emeraldine salt form of PANI is inherently inhomogeneous and phase segregates into oxidized or protonated metallic islands embedded in a sea of insulating material[26]).[27] The charges could not hop to the vicinity of metallic regions, but rather remain confined to the domain of metallic islands.[27] For the T205 and TA05 samples, the ε' shows large negative values on the order of -10^5 starting from 20 to 2 $\times$ 10^3 Hz and it becomes positive at frequencies higher than 2 $\times$ 10^3 Hz. The inset of Fig. 2a shows the relatively stable positive ε' value within the frequency range from 7 $\times$ 10^4 to 2 $\times$ 10^6 Hz. The frequency switch from negative to positive at around 2 $\times$ 10^3 Hz for T205 and 1 $\times$ 10^3 Hz for TA05 is observed. This switching permittivity from negative to positive is also reported in WO_3/PANI nanocomposites and is tuned by controlling the loading and morphology of the WO_3 nanostructures.[17] The ε'' values of pure PANI synthesized by Cr(VI), T205 and TA05 samples, Fig. 2c, exhibit a similar trend as ε'. Pure PANI synthesized by Cr(VI) exhibits a positive ε'' values (from 6.39 $\times$ 10^6 to 85.87), which decreases with increasing frequency. A switching frequency of ε'' from negative to positive is also observed in the T205 and TA05 samples. Fig. 2e shows a frequency dependent tan δ for pure PANI synthesized by Cr(VI), T205 and TA05 samples. The tan δ is observed to decrease with increasing frequency for pure PANI synthesized by Cr(VI). However, for the T205 and TA05 samples, the tan δ increases with increasing frequency from 20 to 2 $\times$ 10^3 and 1 $\times$ 10^3 Hz, respectively, and then decreases with increasing frequency further. The appearance of the peak in the tan δ curve of T205 and TA05 samples is related to the switching of permittivity from negative to positive, which is also observed in polypyrrole/graphene nanocomposites.[13]

Compared with T205 and TA05 samples, T5, T10 and T20 exhibit a negative ε' value, which increases with increasing frequency and the TCr205 shows a very small positive ε' value (<50), which decreases with increasing frequency from 20 to 2 $\times$ 10^6 Hz at room temperature, Fig. 2b. A negative ε' indicates the intrinsic metallic state and disordered motion of the charge carriers along the conjugated polymer backbone,[28] representing the charge delocalization in a macroscopic scale.[6] It is worth noting that the T10 sample has the lowest negative ε' value compared with T5 and T20, providing the highest level of charge delocalization for PANI,[29] which is also observed in the PANI/

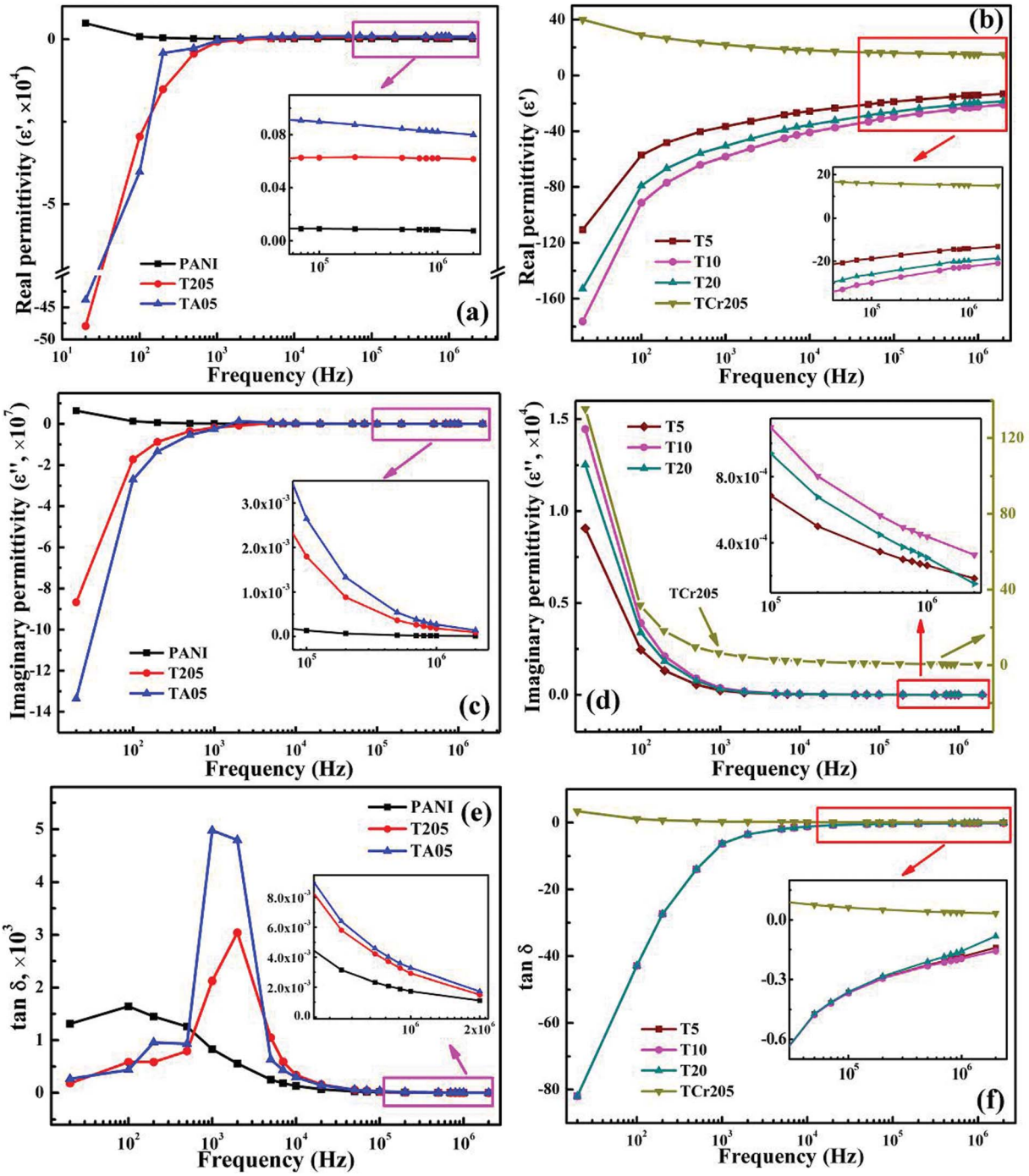

Fig. 2 (a and b) Real permittivity (ε'), (c and d) imaginary permittivity (ε'') and (e and f) dielectric loss tangent (tan δ) as a function of frequency for PANI and MWNTs/PANI nanocomposites.

Fe_3O_4 nanocomposite system with a Fe_3O_4 loading of 16.67 wt %.[6] The difference of the observed negative permittivity in the MWNTs/PANI at different ratios of MWNTs is also observed in WO_3/PANI,[19] $BaTiO_3$/PANI,[8] and Fe_3O_4/PANI nanocomposites.[6] However, the effect of the nanofiller loading on the negative permittivity is still not clear yet. The ε' values for T5, T10 and T20 increase with increasing frequency, which is due to the increased charge carrier polarization.[30] The ε'' significantly decreases with increasing frequency from 20 to 2×10^6 Hz, Fig. 2d. The TCr205 sample shows a small positive ε'' value from 135 to 0.5, whereas the ε'' values of the samples T5, T10 and T20 show a large positive value with a magnitude ranging from 10^5 to 10^1 within the frequency range from 20 to 2×10^6 Hz, Fig. 2d. Generally, the negative permittivity is often explained by the introduced Drude model, which describes the existence and properties of surface plasmons illustrates the frequency dependent permittivity between the external dielectric medium and the surface.[31] In this Drude model, the permittivity is

dominated by plasma-like resonance of the free electrons in a metal, as shown in eqn (1):[16,32]

$$\varepsilon(\omega) = 1 - \frac{Ne^2/(\varepsilon_0 m)}{\omega(\omega + i\gamma)} = 1 - \frac{{\omega_p}^2}{\omega(\omega + i\gamma)} = \left(1 - \frac{{\omega_p}^2}{\omega^2 + \gamma^2}\right) + \left[\frac{{\omega_p}^2\gamma}{\omega(\omega^2 + \gamma^2)}\right] i \quad (1)$$

where $\omega_p \equiv (Ne^2/\varepsilon_0 m)^{1/2} = (4\pi Ne^2/m^*)^{1/2}$ is the plasma frequency and m^* is the optical effective mass of the electron, m is the mass of the electron, e is the charge of the electron, γ stands for the damping constant, ε_0 is the vacuum permittivity, N represents the charge carrier density and ω is the angular frequency of the incident light.[33] From eqn (1), the real part of the permittivity (expressed as $1 - {\omega_p}^2/(\omega^2 + \gamma^2)$) is negative for $\omega < \omega_p$. When the angular frequency is larger than the plasma frequency, the medium behaves as an ordinary dielectric medium.[34]

Fig. 2f depicts the frequency dependent tan δ for the T5, T10, T20 and TCr205 samples. The negative tan δ of the T5, T10 and T20 samples increases with increasing frequency and the magnitude is ranging from -10^2 to -10^{-2} within the frequency range from 20 to 2×10^6 Hz. Interestingly, the T5, T10 and T20 samples are observed to show similar tan δ values, indicating that these three samples have similar energy loss behavior. However, the tan δ of the TCr205 sample decreases with increasing frequency and shows a very small positive value with a magnitude ranging from 10^1 to 10^{-2} within the frequency range from 20 to 2×10^6 Hz. Pure PANI synthesized by Cr(VI), T205 and TA05 samples also show a low positive tan δ value with a magnitude ranging from 10^0 to 10^3 within the measured frequency range, Fig. 2e. The low dielectric loss materials can be applied in radio-frequency and microwave communications.[35]

Fig. 3A and B shows the resistivity as a function of temperature for the as-received MWNTs, pure PANI synthesized by Cr(VI) and MWNTs/PANI nanocomposites. Due to the insulating nature of TCr205, its resistivity is beyond the scope of the used instrument. Typically, the resistivity decreases with increasing temperature for all the synthesized nanocomposites, indicating semiconducting behavior within the measured temperature scale (50–290 K).[36] In this study, the as-received MWNTs show semiconducting behavior, Fig. 3B-d, and the resistivity is decreased from 1.57 Ω cm at 50 K to 1.14 Ω cm at 290 K. The resistivities of TA05 and T205 are lower than that of pure PANI at temperatures from 50 to 290 K and the value varies from 10^1 to 10^3 Ω cm, Fig. 3A-b and c. The resistivities of TA05 and T205 at room temperature are about 26.7 and 5.8 Ω cm. Compared with TA05 and T205 oxidized by APS, very high electrical conductivity (*i.e.* low resistivity) is observed in the T5, T10 and

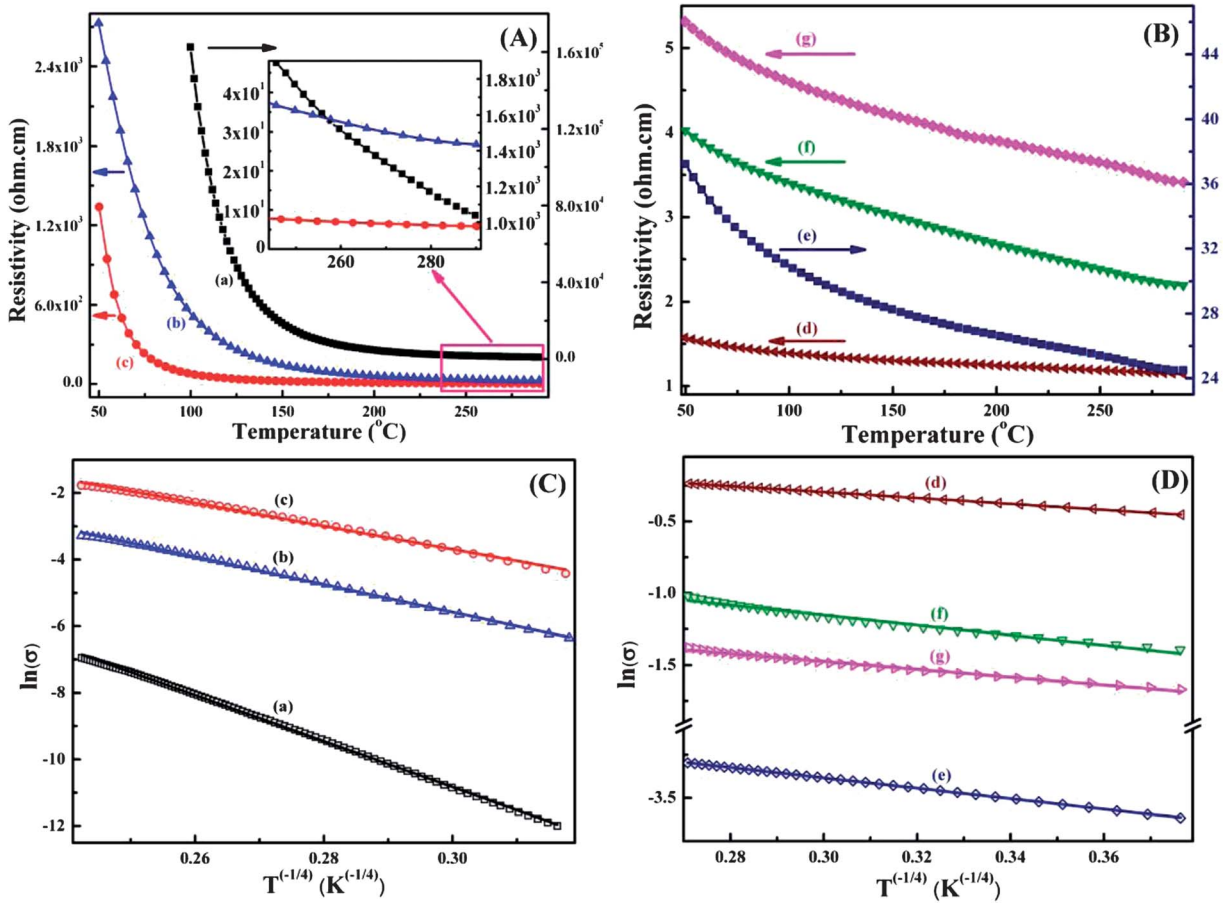

Fig. 3 (A, B) Resistivity *vs.* temperature curves and (C, D) ln (σ) ~ $T^{-1/4}$ curves of (a) pure PANI oxidized by Cr(VI), (b) TA05, (c) T205, (d) as-received MWNTs, (e) T5, (f) T20, and (g) T10 nanocomposites.

T20 nanocomposites oxidized by Cr(VI), Fig. 3B-e, g and f, respectively. For T5, the resistivity is 37.2 Ω cm at 50 K and 24.5 Ω cm at room temperature; and for T10 and T20, the resistivity is changed from 5.3 (50 K) to 3.4 Ω cm (room temperature) and from 4.0 (50 K) to 2.2 Ω cm (room temperature), respectively, Fig. 3B-e, g and f. Generally, the conductive PANI possesses electrical conductivity (σ) ranging from 10^{-2} to 10^{2} S cm^{-1} at room temperature.[37] In this work, pure PANI synthesized by Cr(VI) has very high resistivity from 10^{3} to 10^{5} Ω cm within the measured temperature scale. The room temperature resistivity is about 1.04×10^{3} Ω cm, Fig. 3A-a, which is one order of magnitude higher than that of PANI synthesized by APS (2.06×10^{2} Ω cm).[6] Particularly, previous research has shown that CNTs could be well dispersed in aniline *via* the formation of a donor–acceptor complex.[38] The MWNTs are very good electron acceptors and aniline is a very good electron donor. The interaction between amine groups of aniline and MWNTs renders the MWNTs as conducting bridges, which connect the PANI conducting domains for charge transport causing the observed increased conductivity in the nanocomposites.[39]

The electrical conduction mechanism of the synthesized MWNTs/PANI nanocomposites was investigated by a Mott variable range hopping (VRH) approach, which is presented in eqn (2):[6]

$$\sigma = \sigma_0 \exp\left[-\left(\frac{T_0}{T}\right)^{1/n+1}\right], \quad n = 1,\ 2,\ 3 \tag{2}$$

where the pre-exponential factor σ_0 is a constant, which represents the conductivity at infinite low temperature limit, T is the Kelvin temperature, T_0 is the characteristic Mott temperature and is expressed as eqn (3):[40]

$$T_0 = 24/[\pi k_B N(E_F) a_0{}^3] \tag{3}$$

where a_0 (nm) is the localization length of the localized charge carrier wave function, k_B is the Boltzmann constant and $N(E_F)$ is the density of states at the Fermi level. The n values of 3, 2 and 1 in eqn (2) represent three-, two-, and one-dimensional systems, respectively. σ_0 and T_0 can be calculated from a plot of $\ln(\sigma) \sim T^{-1/n+1}$. For all the measured pressed disc pellet samples, the temperature dependent resistivity follows a linear relationship of $\ln(\sigma)$ *vs.* $T^{-1/4}$, Fig. 3C and D, indicating a quasi-3-dimensional VRH hopping mechanism. This means that all the samples are disordered systems in the 3-dimensional VRH regime. These results are very similar to synthesized Fe_3O_4/PANI[6] and WO_3/PANI[19] nanocomposites. The σ_0 and T_0 obtained from Fig. 3C and D are summarized in Table 1. The as-received MWNTs show the lowest T_0 value of 17.75 K and pure PANI shows the highest T_0 value of 2.20×10^{7} K. Generally, a larger T_0 indicates a stronger localization of the charge carriers in the system (*i.e.* disordered system) and a lower T_0 indicates a weaker localization.[41] The higher T_0 will cause stronger scattering, leading to a higher resistivity.[6] In this work, the T_0 value of the MWNTs/PANI nanocomposites obeys the following order: T20 < T10 < T5 < T205 < TA05, which is consistent with the measured resistivity values. This order also shows that the T_0 of the nanocomposites synthesized by Cr(VI) is lower than that of the nanocomposites synthesized by APS.

Table 1 T_0 and σ_0 for the as-received MWNTs, synthesized PANI and MWNTs/PANI nanocomposites

Sample	T_0 (K)	σ_0 (S cm^{-1})
As-received MWNTs	17.75	1.378
PANI	2.20×10^{7}	17 331
T5	78.20	0.083
T10	68.12	0.729
T20	41.10	0.485
T205	1.61×10^{6}	1121
TA05	3.10×10^{6}	1112

Fig. 4A displays the magnetic field (H) dependent magnetoresistance (MR) for the as-received MWNTs, pure PANI synthesized by Cr(VI) and MWNTs/PANI nanocomposites at room temperature. The MR is defined as the ratio in eqn (4):

$$\mathrm{MR} = \Delta R/R = [R(H) - R(0)]/R(0) \tag{4}$$

where $R(H)$ is the resistance of a material under a magnetic field H and $R(0)$ is the resistance without any magnetic field. The as-received MWNTs have shown a small positive MR of around 2.4% at $H = 9$ T, Fig. 4A-d. The pure PANI synthesized by Cr(VI) shows a positive MR of around 3.6% at $H = 9$ T, Fig. 4A-c. It is interesting to observe that the T5 (Fig. 4A-e) and T20 (Fig. 4A-f) nanocomposites exhibit negative MR within the entire magnetic field range and the MR values are found to be −2.11 and −1.99% at $H = 9$ T, respectively, however, the T205 (Fig. 4A-a) and TA05 (Fig. 4A-b) nanocomposites exhibit positive MR in the measured magnetic field range and the MR values are around 11.1 and 7.9% at $H = 9$ T, respectively. The MR value of TA05 is lower than that of the MWNTs/PANI nanocomposites with the same MWNTs loading synthesized by APS *via* sonication method (around 15% at $H = 9$ T).[9] These room temperature MR values are relatively higher than other organic systems, such as only 0.3% MR obtained in the $La_{0.7}Sr_{0.3}MnO_3$/poly(3-hexylthiophene-2,5-diyl) system at 300 K.[42]

Generally, the MR of highly disordered localized systems in the VRH regime can be described using the orbital magnetoconductivity theory (also called forward interference model) and wave-function shrinkage model.[43] In the temperature dependent resistivity section, pure PANI synthesized by Cr(VI) and its MWNTs nanocomposites are confirmed to be disordered systems in the 3-dimensional VRH regime. Therefore, these two numerical models can be applied to pure PANI synthesized by Cr(VI) and its MWNT nanocomposites. In the wave-function shrinkage model, the contraction of the electronic wave-function at impurity centers in a magnetic field was considered and the $R(H,T)/R(0,T)$ can be expressed according to eqn (5):[44]

$$R(H,T)/R(0,T) = \exp\{\xi_C(0)[\xi_C(H)/\xi_C(0) - 1]\} \tag{5}$$

where $\xi_C(0) = (T_0/T)$ for the 3-d Mott VRH electrical conduction mechanism, $\xi_C(H)/\xi_C(0)$ is the normalized hopping probability parameter and is a function of H/P_C for the Mott VRH electrical

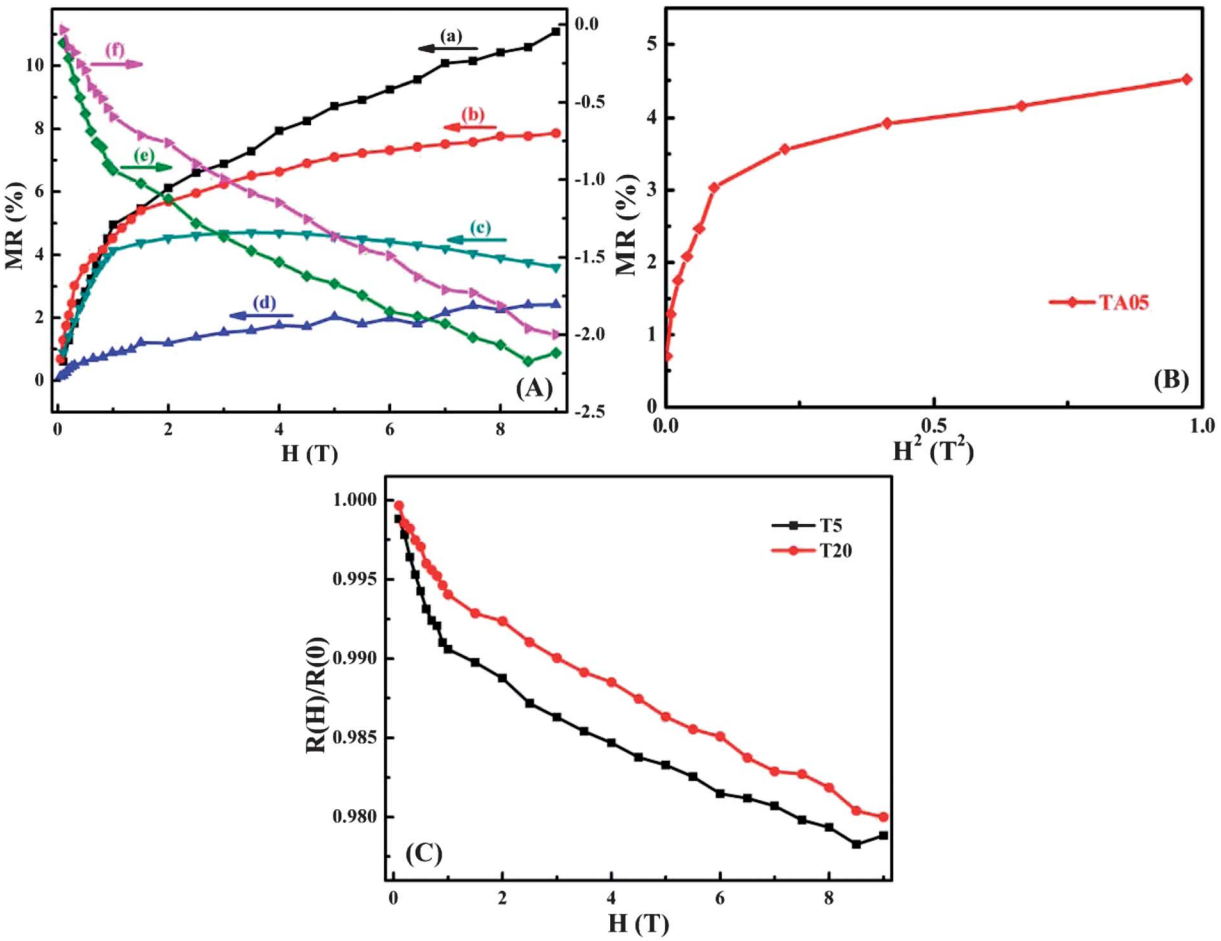

Fig. 4 (A) Magnetoresistance of (a) T205, (b) TA05, (c) PANI synthesized by Cr(VI), (d) as-received MWNTs, (e) T5, and (f) T20 at $T = 290$ K; (B) MR as a function of H^2 for the TA05 sample; and (C) ratio $R(H)/R(0)$ as a function of H for T5 and T20 samples.

conduction mechanism. H is the magnetic field, P_C is the fitting parameter, which is the normalized characteristic magnetic field and can be given by eqn (6) for the 3-dimensional Mott VRH system:[7]

$$P_C = 6\hbar/[ea_0{}^2(T_0/T)^{1/4}] \quad (6)$$

where e is electron charge, $\hbar$ is the reduced Planck's constant, and T_0 is the Mott characteristic temperature (K). In the low magnetic field limit, eqn (5) is simplified to eqn (7):[45]

$$R(H,T)/R(0,T) \approx 1 + t_2\frac{H^2}{P_C{}^2}\left(\frac{T_0}{T}\right)^{1/4} \quad (7)$$

And the MR is defined in eqn (8):

$$\mathrm{MR} = \frac{R(H,T) - R(0,T)}{R(0,T)} \approx t_2\frac{H^2}{P_C{}^2}\left(\frac{T_0}{T}\right)^{1/4} = t_2\frac{e^2a_0{}^4}{36\hbar^2}\left(\frac{T_0}{T}\right)^{3/4}H^2 \quad (8)$$

where the numerical constant $t_2 = 5/2016$.[7] From eqn (8), it can be concluded that the MR value obtained from wave-function shrinkage model is always positive, thus, it is often used to explain the positive MR value. According to eqn (8), in the wave-function shrinkage model, the localization length a_0 can be expressed from the slope of the curve by plotting $\mathrm{MR} \sim H^2\left(k = t_2\frac{e^2a_0{}^4}{36h^2}\left(\frac{T_0}{T}\right)^{3/4}\right)$. For example, the representative curve MR $\sim H^2$ for the TA05 sample is shown in Fig. 4B. The slope of curve MR $\sim H^2$ for the TA05 sample becomes lower and lower with increasing H^2, which means that the localization length a_0 will be reduced as H increases. Meanwhile, the localization length a_0 can be calculated by using eqn (9) from T_0, positive MR value and H:

$$a_0{}^4 = \frac{36h^2\mathrm{MR}}{t_2e^2}\left(\frac{T_0}{T}\right)^{-3/4}H^{-2} \quad (9)$$

The obtained localization lengths a_0 at different H for the samples with a positive MR value are listed in Table 2. From Table 2, a_0 is observed to have the magnetic field dependent behavior and decreases with increasing magnetic field. As aforementioned, the density of states at the Fermi level $N(E_F)$ can be calculated from eqn (10) according to eqn (3):

$$N(E_F) = 24/[\pi k_B T_0 a_0{}^3] \quad (10)$$

Table 2 a_0, $N(E_F)$ and R_{hop} for PANI synthesized by Cr(VI) and its MWNTs nanocomposites at different H

		Magnetic field H (T)		
Sample	Parameter	0.1	0.5	1.0
PANI	a_0 (nm)	62.1	25.2	15.7
synthesized	$N(E_F)$ (J cm^3)$^{-1}$	1.1×10^{32}	1.6×10^{33}	6.5×10^{33}
by Cr(VI)	R_{hop} (μm)	0.387	0.157	0.098
T205	a_0 (nm)	102.6	46.9	34.0
	$N(E_F)$ (J cm^3)$^{-1}$	3.2×10^{32}	3.3×10^{33}	8.7×10^{33}
	R_{hop} (nm)	0.332	0.152	0.110
TA05	a_0 (nm)	96.1	39.7	27.6
	$N(E_F)$ (J cm^3)$^{-1}$	2.0×10^{32}	2.9×10^{33}	8.5×10^{33}
	R_{hop} (μm)	0.366	0.151	0.105

The calculated $N(E_F)$ values are also listed in Table 2. Normally, the hopping probability between the localized states increases with increasing $N(E_F)$,[46] which means that the higher the $N(E_F)$, the larger the hopping probability of the charge carriers will be.[7] The average hopping length R_{hop} can be obtained by using eqn (11):

$$R_{hop} = (3/8)(T_0/T)^{1/4} a_0 \quad (11)$$

The obtained R_{hop} (μm) is shown in Table 2 and the R_{hop} is observed to decrease with increasing H. Generally, the MR in the hopping system is due to the contraction of the charge carrier wave- function and the subsequent reduced average hopping length.[9]

The orbital magnetoconductivity theory is normally used to predict the negative MR values. The effect of interference among various hopping paths was considered in this theory. These hopping paths include sequence of scattering of tunneling charge carriers by the impurities located within a cigar-shaped domain of length R_{hop} (hopping length) and width $(R_{hop}\, a_0)^{1/2}$.[44] The ratio $R(H,T)/R(0,T)$ caused by the interference effects is described by empirical eqn (12), which neglects the quadratic term in H:[47–49]

$$R(H,T)/R(0,T) \approx 1/\{1 + C_{sat}[H/H_{sat}]/[1 + H/H_{sat}]\} \quad (12)$$

where the fitting parameter C_{sat} is a constant and the other fitting parameter H_{sat} is the effective magnetic field to saturate the MR. The obtained ratio $R(H)/R(0)$ as a function of H is shown in Fig. 4C. By fitting $R(H)/R(0) \sim H$ *via* eqn (12) using Polymath software, the obtained C_{sat} values for T5 and T20 are 0.0251127 and 0.0317174, respectively.

For the Mott VRH electrical conduction mechanism is given by eqn (13):[7]

$$H_{sat} \approx 0.7\left(\frac{8}{3}\right)^{3/2}\left(\frac{1}{a_0{}^2}\right)\left(\frac{h}{e}\right)\left(\frac{T}{T_0}\right)^{3/8} \quad (13)$$

where h is Planck's constant, e is electron charge and T_0 is the Mott characteristic temperature (K). In the low-field limit, eqn (12) becomes eqn (14):

$$R(H,T)/R(0,T) \approx 1 - C_{sat}[H/H_{sat}] \quad (14)$$

Substituting eqn (13) into eqn (14) and rearranging, the obtained MR is as eqn (15):

$$\mathrm{MR} = \frac{\Delta R(H,T) - R(0,T)}{R(0,T)} \approx -C_{sat}[H/H_{sat}] = -C_{sat}\frac{H}{0.7\left(\frac{8}{3}\right)^{3/2}\left(\frac{1}{a_0{}^2}\right)\left(\frac{h}{e}\right)\left(\frac{T}{T_0}\right)^{3/8}} \quad (15)$$

The calculated a_0 values for T5 *via* eqn (14) are 0.989, 0.970 and 0.879 μm at H of 0.3, 0.5 and 1.0 T, respectively. The obtained a_0 for the T5 and T20 samples at different H according to eqn (14) are listed in Tables S1 and S2,† respectively. It is observed that the a_0 for the negative MR value in the T5 sample is larger than that of the positive MR value in the T205 and TA05 samples at the same magnetic field. The large a_0 for the negative MR value is also observed in magnetite/polypyrrole nanocomposites.[50]

In conclusion, MWNTs/PANI nanocomposites have been synthesized by using the SIP method with Cr(VI) as the oxidant and compared with MWNTs/PANI nanocomposites prepared with APS as oxidant. The obtained as-received MWNTs, pure PANI synthesized by Cr(VI) and MWNTs/PANI nanocomposites are observed to follow a quasi-3-d VRH electrical conduction mechanism. Negative permittivity is observed in the MWNTs/PANI nanocomposites synthesized by Cr(VI), however, a switching frequency, in which the permittivity changes from negative to positive, is observed in the MWNTs/PANI nanocomposites synthesized by APS. A negative GMR around −2% is observed in the MWNTs/PANI nanocomposites synthesized by Cr(VI), a positive GMR about 2.4% is observed in the as-received MWNTs, around 4% for pure PANI synthesized by Cr(VI), 7.9 and 11% in the TA05 and T205 nanocomposites synthesized by APS. The observed positive and negative GMR effects have been well explained by the calculated localization length (a_0) based on the wave-function shrinkage model and orbital magnetoconductivity theory, respectively. The obtained a_0 for the negative MR value in the MWNT/PANI nanocomposites with Cr(VI) as oxidant is larger than that of the positive MR value in the nanocomposites T205 formed with further APS as oxidant and nanocomposites TA05 formed with APS as oxidant at the same magnetic field.

Acknowledgements

This project is financially supported by the National Science Foundation Nanoscale Interdisciplinary Research Team, and Materials Processing and Manufacturing (CMMI 10-30755). D. P. Young acknowledges support from the NSF under grant no. DMR 13–06392. The Raman spectra were collected at the Materials Characterization Facility at Texas A&M University by Dr Amanda Young. H. Gu acknowledges the support from China Scholarship Council (CSC) program.

Notes and references

1 M. N. Baibich, J. M. Broto, A. Fert, F. N. Van Dau, F. Petroff, P. Etienne, G. Creuzet, A. Friederich and J. Chazelas, *Phys. Rev. Lett.*, 1988, **61**, 2472–2475.

2 L. Bogani and W. Wernsdorfer, *Nat. Mater.*, 2008, **7**, 179–186.
3 P. Gao, D. Beckmann, H. N. Tsao, X. Feng, V. Enkelmann, M. Baumgarten, W. Pisula and K. Müllen, *Adv. Mater.*, 2009, **21**, 213–216.
4 V. Y. Aristov, O. V. Molodtsova, Y. A. Ossipyan, B. P. Doyle, S. Nannarone and M. Knupfer, *Org. Electron.*, 2009, **10**, 8–11.
5 Y. Ohno, K. Narumi, K. Maehashi, K. Inoue and K. Matsumoto, *J. Phys. Conf. Ser.*, 2006, **38**, 57–60.
6 H. Gu, Y. Huang, X. Zhang, Q. Wang, J. Zhu, L. Shao, N. Haldolaarachchige, D. P. Young, S. Wei and Z. Guo, *Polymer*, 2012, **53**, 801–809.
7 H. Gu, J. Guo, X. Zhang, Q. He, Y. Huang, H. A. Colorado, N. S. Haldolaarachchige, H. L. Xin, D. P. Young, S. Wei and Z. Guo, *J. Phys. Chem. C*, 2013, **117**, 6426–6436.
8 X. Zhang, S. Wei, N. Haldolaarachchige, H. A. Colorado, Z. Luo, D. P. Young and Z. Guo, *J. Phys. Chem. C*, 2012, **116**, 15731–15740.
9 J. Zhu, H. Gu, Z. Luo, N. Haldolaarachige, D. P. Young, S. Wei and Z. Guo, *Langmuir*, 2012, **28**, 10246–10255.
10 S.-B. Yoon, E.-H. Yoon and K.-B. Kim, *J. Power Sources*, 2011, **196**, 10791–10797.
11 T. Yang, N. Zhou, Y. Zhang, W. Zhang, K. Jiao and G. Li, *Biosens. Bioelectron.*, 2009, **24**, 2165–2170.
12 M. U. Jurczyk, A. Kumar, S. Srinivasan and E. Stefanakos, *Int. J. Hydrogen Energy*, 2007, **32**, 1010–1015.
13 H. Gu, S. Tadakamalla, X. Zhang, Y.-D. Huang, Y. Jiang, H. A. Colorado, Z. Luo, S. Wei and Z. Guo, *J. Mater. Chem. C*, 2013, **1**, 729–743.
14 R. W. Ziolkowski and E. Heyman, *Phys. Rev. E: Stat., Nonlinear, Soft Matter Phys.*, 2001, **64**, 056625.
15 D. R. Smith, J. B. Pendry and M. C. K. Wiltshire, *Science*, 2004, **305**, 788–792.
16 H. Gu, J. Guo, S. Wei and Z. Guo, *J. Appl. Polym. Sci.*, 2013, **130**(4), 2238–2244.
17 J. Zhu, S. Wei, L. Zhang, Y. Mao, J. Ryu, P. Mavinakuli, A. B. Karki, D. P. Young and Z. Guo, *J. Phys. Chem. C*, 2010, **114**, 16335–16342.
18 H. Gu, S. Rapole, J. Sharma, Y. Huang, D. Cao, H. A. Colorado, Z. Luo, N. Haldolaarachchige, D. P. Young, S. Wei and Z. Guo, *RSC Adv.*, 2012, **2**, 11007–11018.
19 J. Zhu, S. Wei, L. Zhang, Y. Mao, J. Ryu, A. B. Karki, D. P. Young and Z. Guo, *J. Mater. Chem.*, 2011, **21**, 342–348.
20 M. G. Han, S. K. Cho, S. G. Oh and S. S. Im, *Synth. Met.*, 2002, **126**, 53–60.
21 Y. C. Jung, H. H. Kim, Y. A. Kim, J. H. Kim, J. W. Cho, M. Endo and M. S. Dresselhaus, *Macromolecules*, 2010, **43**, 6106–6112.
22 D. McIntosh, V. N. Khabashesku and E. V. Barrera, *J. Phys. Chem. C*, 2007, **111**, 1592–1600.
23 M. L. Shofner, V. N. Khabashesku and E. V. Barrera, *Chem. Mater.*, 2006, **18**, 906–913.
24 D. McIntosh, V. N. Khabashesku and E. V. Barrera, *Chem. Mater.*, 2006, **18**, 4561–4569.
25 J. Zhu, M. Chen, H. Qu, X. Zhang, H. Wei, Z. Luo, H. A. Colorado, S. Wei and Z. Guo, *Polymer*, 2012, **53**, 5953–5964.
26 H. L. Wu and P. Phillips, *Phys. Rev. Lett.*, 1991, **66**, 1366–1369.
27 J. Joo, E. J. Oh, G. Min, A. G. MacDiarmid and A. J. Epstein, *Synth. Met.*, 1995, **69**, 251–254; J. Zhu, X. Zhang, N. Haldolaarachchige, Q. Wang, Z. Luo, J. Ryu, D. P. Young, S. Wei and Z. Guo, *J. Mater. Chem.*, 2012, **22**, 4996–5005; X. Zhang, J. Zhu, N. Haldolaarachchige, J. Ryu, D. P. Young, S. Wei and Z. Guo, *Polymer*, 2012, **53**, 2109–2120.
28 C. D. Liu, S. N. Lee, C. H. Ho, J. L. Han and K. Hsieh, *J. Phys. Chem. C*, 2008, **112**, 15956–15960.
29 A. K. Singh, T. C. Goel, R. G. Mendiratta, O. P. Thakur and C. Prakash, *J. Appl. Phys.*, 2002, **91**, 6626–6629.
30 J. Homola, *Chem. Rev.*, 2008, **108**, 462–493.
31 J. B. Pendry, A. J. Holden, W. J. Stewart and I. Youngs, *Phys. Rev. Lett.*, 1996, **76**, 4773–4776.
32 M. Rashidi-Huyeh and B. Palpant, *Phys. Rev. B: Condens. Matter Mater. Phys.*, 2006, **74**, 075405.
33 F. Capolino, *Theory and Phenomena of Metamaterials*, CRC Press, 2009.
34 N. M. Alford and S. J. Penn, *J. Appl. Phys.*, 1996, **80**, 5895–5898.
35 S. Chakrabarti, D. Banerjee and R. Bhattacharyya, *J. Phys. Chem. B*, 2002, **106**, 3061–3064.
36 J. Stejskal, I. Sapurina, M. Trchová, J. Prokeš, I. Křivka and E. Tobolková, *Macromolecules*, 1998, **31**, 2218–2222.
37 Y. Sun, S. R. Wilson and D. I. Schuster, *J. Am. Chem. Soc.*, 2001, **123**, 5348–5349.
38 X.-h. Li, B. Wu, J.-e. Huang, J. Zhang, Z.-f. Liu and H.-l. Li, *Carbon*, 2003, **41**, 1670–1673.
39 L. Zhang and Z.-J. Tang, *Phys. Rev. B: Condens. Matter Mater. Phys.*, 2004, **70**, 174306.
40 J. Zhu, S. Wei, L. Zhang, Y. Mao, J. Ryu, A. B. Karki, D. P. Young and Z. Guo, *J. Mater. Chem.*, 2011, **21**, 342–348.
41 M. Aggarwal, S. Khan, M. Husain, T. Ming, M. Tsai, T. Perng and Z. Khan, *Eur. Phys. J. B*, 2007, **60**, 319–324.
42 A. Ozbay, E. R. Nowak, Z. G. Yu, W. Chu, S. Yijian, S. Krishnamurthy, Z. Tang and N. Newman, *Appl. Phys. Lett.*, 2009, **95**, 232507.
43 H. Gu, X. Zhang, H. Wei, Y. Huang, S. Wei and Z. Guo, *Chem. Soc. Rev.*, 2013, **42**, 5907–5943.
44 T.-I. Su, C.-R. Wang, S.-T. Lin and R. Rosenbaum, *Phys. Rev. B: Condens. Matter Mater. Phys.*, 2002, **66**, 054438.
45 H. Gu, J. Guo, H. We, Y. Huang, C. Zhao, Y. Li, Q. Wu, N. Haldolaarachchige, D. P. Young, S. Wei and Z. Guo, *Phys. Chem. Chem. Phys.*, 2013, **15**, 10866–10875.
46 K. Dutta and S. K. De, *Phys. Lett. A*, 2007, **361**, 141–145.
47 U. Sivan, O. Entin-Wohlman and Y. Imry, *Phys. Rev. Lett.*, 1988, **60**, 1566–1569.
48 R. Rosenbaum, A. Milner, S. Hannahs, T. Murphy, E. Palm and B. Brandt, *Phys. B*, 2001, **294–295**, 340–342.
49 O. Entin-Wohlman, Y. Imry and U. Sivan, *Phys. Rev. B: Condens. Matter Mater. Phys.*, 1989, **40**, 8342–8348.
50 J. Guo, H. Gu, H. Wei, Q. Zhang, N. S. Haldolaarachchige, Y. Li, D. P. Young, S. Wei and Z. Guo, *J. Phys. Chem. C*, 2013, **117**, 10191–10202.